



Cite as

Nano-Micro Lett.

(2020) 12:72

Potential of MXenes in Water Desalination: Current Status and Perspectives

Ihsanullah Ihsanullah¹ ✉

Received: 29 December 2019

Accepted: 7 February 2020

© The Author(s) 2020

✉ Ihsanullah Ihsanullah, engr.ihsan.dir@gmail.com; ihsankhan@kfupm.edu.sa

¹ Center for Environment and Water, Research Institute, King Fahd University of Petroleum and Minerals, Dhahran 31261, Saudi Arabia

HIGHLIGHTS

- A broad overview of MXenes and MXene-based nanomaterials in desalination is presented.
- Recent advancement in the synthesis of MXenes for applications in desalination is critically evaluated. Salt removal mechanisms and regeneration capability of MXenes are appraised.
- Current challenges and future prospect of MXenes in desalination are highlighted. Research directions are provided to safeguard the applications of MXenes in future desalination.

ABSTRACT MXenes, novel 2D transition metal carbides, have emerged as wonderful nanomaterials and a superlative contestant for a host of applications. The tremendous characteristics of MXenes, i.e., high surface area, high metallic conductivity, ease of functionalization, biocompatibility, activated metallic hydroxide sites, and hydrophilicity, make them the best aspirant for applications in energy storage, catalysis, sensors, electronics, and environmental remediation. Due to their exceptional physicochemical properties and multifarious chemical compositions, MXenes have gained considerable attention for applications in water treatment and desalination in recent times. It is vital to understand the current status of MXene applications in desalination in order to define the roadmap for the development of MXene-based materials and endorse their practical applications in the future. This paper critically reviews the recent advancement in the synthesis of MXenes and MXene-based composites for applications in desalination. The desalination potential of MXenes is portrayed in detail with a focus on ion-sieving membranes, capacitive deionization, and solar desalination. The ion removal mechanism and regeneration ability of MXenes are also summarized to get insight into the process. The key challenges and issues associated with the synthesis and applications of MXenes and MXene-based composites in desalination are highlighted. Lastly, research directions are provided to guarantee the synthesis and applications of MXenes in a more effective way. This review may provide an insight into the applications of MXenes for water desalination in the future.



KEYWORDS MXenes; 2D materials; Metal carbides; Capacitive deionization; Solar desalination; Water desalination



1 Introduction

MXenes (pronounced “maxines”), a new family of 2D transition metal carbides, nitrides, and carbonitrides, were discovered by researchers at Drexel University in 2011 [1–4]. The first-ever MXene comprised of 2D titanium carbide (Ti_3C_2) was synthesized by selectively etching the “A” (Al atoms) in layered hexagonal ternary carbide, Ti_3AlC_2 , with hydrofluoric acid (HF) at room temperature [1]. MXenes are represented by the general formula $\text{M}_{n+1}\text{X}_n\text{T}_x$ ($n = 1\text{--}3$) and are derived from the precursor MAX phase ($\text{M}_{n+1}\text{AX}_n$), where M is an early transition metal, X is carbon and/or nitrogen, A represents an element from groups 12 to 16, T denotes the surface termination groups such as fluorine (–F), oxygen (=O), chlorine (–Cl), and hydroxyl (–OH), and x represents the number of surface functionalities [2, 5–13]. In the MAX phase, A layer is sandwiched within octahedral M_{n+1}X_n , with strong M–X bond and relatively weak M–A bond [14–16]. MAX phases ($\text{M}_{n+1}\text{AX}_n$) forming elements of the periodic table are highlighted in Fig. 1 [17]. The interlayer spacing of MXenes is usually in the

range of 1 nm and is dependent on the value of n in MXenes ($\text{M}_{n+1}\text{X}_n\text{T}_x$) [13].

So far, nearby 30 MXenes compositions are reported in the literature that have been synthesized from the MAX phase precursors primarily by incorporating two or more transition metals in the M layers [5, 18–21]. Among them, titanium-based MXenes (such as $\text{Ti}_3\text{C}_2\text{T}_x$ and Ti_2CT_x) are extensively employed in environmental applications [1, 18]. Besides carbides, other MXenes structures with nitride and carbonitride have also been employed in various fields [19, 22–25]. Owing to their unique layered structures and 2D morphology, MXenes can be easily exploited to form a composite with other materials to enhance their properties [25–30].

MXenes have arisen a significant consideration of scientists and academicians due to their fascinating chemical, mechanical, electronic, and magnetic properties [18]. The incredible features of MXenes including, but not limited to, high surface area, environmentally friendly nature, biocompatibility, activated metallic hydroxide sites, ease of functionalization, antibacterial properties, high

hydrogen 1 H 1.0079																	helium 2 He 4.0026	
lithium 3 Li 6.941	beryllium 4 Be 9.0122																	neon 10 Ne 20.180
sodium 11 Na 22.990	magnesium 12 Mg 24.305																	argon 18 Ar 39.948
potassium 19 K 39.098	calcium 20 Ca 40.078	scandium 21 Sc 44.956	titanium 22 Ti 47.867	vanadium 23 V 50.942	chromium 24 Cr 51.996	manganese 25 Mn 54.938	iron 26 Fe 55.845	cobalt 27 Co 58.933	nickel 28 Ni 58.693	copper 29 Cu 63.546	zinc 30 Zn 65.38	boron 5 B 10.811	carbon 6 C 12.011	nitrogen 7 N 14.007	oxygen 8 O 15.999	fluorine 9 F 18.998	helium 10 He 4.0026	
rubidium 37 Rb 85.468	strontium 38 Sr 87.62	yttrium 39 Y 88.906	zirconium 40 Zr 91.224	niobium 41 Nb 92.906	molybdenum 42 Mo 95.94	technetium 43 Tc [98]	ruthenium 44 Ru 101.07	rhodium 45 Rh 102.91	palladium 46 Pd 106.42	silver 47 Ag 107.87	cadmium 48 Cd 112.41	aluminum 13 Al 26.982	silicon 14 Si 28.086	phosphorus 15 P 30.974	sulfur 16 S 32.065	chlorine 17 Cl 35.453	argon 18 Ar 39.948	
cesium 55 Cs 132.91	barium 56 Ba 137.33	hafnium 72 Hf 178.49	tantalum 73 Ta 180.95	tungsten 74 W 183.84	rhenium 75 Re 186.21	osmium 76 Os 190.23	iridium 77 Ir 192.22	platinum 78 Pt 195.08	gold 79 Au 196.97	mercury 80 Hg 200.59	indium 49 In 114.82	tin 50 Sn 118.71	antimony 51 Sb 121.76	tellurium 52 Te 127.60	iodine 53 I 126.90	xenon 54 Xe 131.29	radon 86 Rn [222]	
francium 87 Fr [223]	radium 88 Ra [226]	rutherfordium 104 Rf [261]	dubnium 105 Db [262]	seaborgium 106 Sg [266]	bohrium 107 Bh [264]	hassium 108 Hs [277]	meitnerium 109 Mt [268]	darmstadtium 110 Ds [271]	roentgenium 111 Rg [272]									

Fig. 1 Elements in the periodic table that are known to form $\text{M}_{n+1}\text{AX}_n$ phases. Reprinted with the permission from Ref. [17]. Copyright © (2019) Elsevier Ltd and Techna Group S.r.l

metallic conductivity, and hydrophilicity make them an ideal candidate for various applications such as environmental remediation, energy storage, electronics, sensors, and catalysis [6, 14, 16, 28, 31, 32]. The exceptional electrical conductivity ($\sim 6500 \text{ S m}^{-1}$) and high surface area of MXenes (up to $347 \text{ m}^2 \text{ g}^{-1}$) are essential characteristics for their applications in conductive films, electrical measurements, adsorption, and energy storage [6, 13, 33]. Recent studies demonstrated that MXenes also holds a prominent future in water splitting applications [34, 35]. MXenes have also been studied as an emerging material for application in water purification, i.e., capacitive deionization, membranes, and adsorption [36–45].

This review is focused on the evaluation of MXenes and MXene-based composites for applications in desalination. The desalination potential of MXenes is portrayed in detail with an emphasis on ion-sieving membranes, capacitive deionization, and solar desalination. The key challenges and issues allied with the synthesis and applications of MXenes and MXene-based composites in desalination are highlighted. Future research directions are provided to guarantee the efficient synthesis and applications of MXenes in desalination.

2 Desalination Potential of MXenes

MXenes and their composites have demonstrated a substantial potential in numerous environmental applications such as adsorption, membrane separations, and capacitive deionization. MXenes are promising aspirants for water purification membranes owing to their hydrophilicity, high surface area, and excellent mechanical and electrical properties [46–48]. MXenes and MXene-based composites are favorable candidates in desalination applications. MXene ($\text{Ti}_3\text{C}_2\text{T}_x$) has a low contact angle of 21.5° , and it exhibited excellent stability in water even after vigorous shaking that makes them an ideal candidate for desalination applications [49].

2.1 Ion-Sieving Membranes

MXene nanosheets can be employed for rejection of size- and charge-selective rejection of molecules and ions either in freestanding or supported membranes. Performance evaluation of different MXene membranes for potential

applications in desalination is presented in Table 1. Molecules can be separated via size exclusion through the stacked layers and by interaction with the charged MXene layers. Smaller ions from water can be eliminated due to constrained interlayer spacing of MXenes. The water flux through MXene ($\text{Ti}_3\text{C}_2\text{T}_x$)-based membranes was high, and the membranes exhibited excellent separation potential for various ions based on charge and hydration radius of the ion [36, 50].

Ren et al. [36] fabricated the $\text{Ti}_3\text{C}_2\text{T}_x$ membrane by a vacuum-assisted filtration (VAF) method (Fig. 2) and reported the selective sieving of various cations through the membrane. The thickness of the membrane played a crucial role in water permeation through the membrane. The flux through the MXene membrane declined with increasing thickness until reaching a steady-state value at higher thickness. MXene membrane exhibited an ultrafast water flux $\sim 38 \text{ L (m}^2 \text{ h bar)}^{-1}$ at the membrane thickness of 1500 nm.

As depicted in Fig. 3, the interlayer distances of the $\text{Ti}_3\text{C}_2\text{T}_x$ membranes expedite the fast flow of water. The permeation rates of alkali, alkaline earth (Li^+ , Na^+ , K^+ , Mg^{2+} , and Ca^{2+}), transition and other metal (Ni^{2+} and Al^{3+}), and methylthionium⁺ (MB^+) dye cations followed the order: $\text{Na}^+ > \text{Li}^+ > \text{K}^+ > \text{Ca}^{2+} > \text{Ni}^{2+} > \text{Mg}^{2+} > \text{Al}^{3+} \gg \text{MB}^+$. The permeation was found dependent on both the cations' size and charge. Single-charged Na^+ or K^+ ions were found to intercalate readily into the MXene membrane compared to the double-charged Mg^{2+} ions and bulky ions such as Al^{3+} . MXene membranes show better selectivity toward charged metal cations and dye cations of different sizes than graphene oxide [36].

Cations with larger radii than the interlayer distance ($\sim 6.4 \text{ \AA}$) are debarred based on size. Cations with radii smaller than the interlayer distance can penetrate into the interlayer capillary pathways and increase the interlayer spacing. However, when abundant ions are intercalated, the electrostatic attraction between the charged ions and negatively charged MXene surface results in shrinkage of the layers. Finally, single-charged ions (Na^+) can pass through the membrane and are attracted to each side of MXene layers, forming an electric double layer on the surface and causing expansion of $\text{Ti}_3\text{C}_2\text{T}_x$ interlayer spacing. The actuation mechanism explains the cations permeation and high flux of Na^+ due to increasing the interlayer spacing. On the other



Table 1 Ion sieving performance evaluation of different MXene membranes

Membrane	Rejection (%)	Permeability (L/m ² h bar)	Remarks	References
MXene-derived membranes supported on α -Al ₂ O ₃	Na ₂ SO ₄ : 75.9 MgSO ₄ : 67.3 NaCl: 55.3 MgCl ₂ : 46.1	22.4 L	The interlayer spacing between nanosheets of MXene-derived membranes can be adjusted by regulating the sintering temperature The interlayer spacing decreased with an increase in temperature At temperature > 400 °C, the oxidation of Ti ₃ C ₂ T _x nanosheets into TiO ₂ NPs occurs and the ion retention reduced	[54]
Ti ₃ C ₂ T _x membrane	–	38	The flux through MXene membrane declined with increasing thickness until reaching a steady-state value at higher thickness The permeation was found dependent on both the cations' size and charge Better selectivity is shown toward charged metal cations and dye cations of different sizes than GO	[36]
Ag@MXene composite membrane	MG: 92.32 RhB: 79.93 BSA: 100 NaCl: 25.8 MgCl ₂ : 41.3 AlCl ₃ : 49.5	420	Ag@MXene membrane demonstrated higher water flux than pristine MXene membranes Ag@MXene composite membrane also revealed enhanced bactericidal characteristics and moderate salt rejection	[51]
MXene membrane supported on anodic aluminum oxide (AAO) substrate	BSA: 100 RB, Rhodamine B: 85 EB, Evans Blue: 90 Cytochrome C: 97	1084	Membrane exhibited high water flux (> 1000 L/m ² h bar) and promising rejection rate (> 90 %) for molecules with sizes larger than 2.5 nm The improved water permeation can be attributed to the additional nanochannels formed in the MXene membrane after deposition on AAO support	[53]
Self-cross-linked MXene (Ti ₃ C ₂ T _x) membranes	NaCl: 98.6	0.0515	Self-cross-linked MXene membrane exhibited excellent stability and anti-swelling property Membrane demonstrated improved performance of the ion exclusion compared to pristine MXene	[57]
Ti ₃ C ₂ T _x	MB: 98.0 ± 0.9	10.6	Positive and negative voltages decreased and increased rejection through MXene membranes, respectively Exclusion of ions from the Ti ₃ C ₂ T _x membranes by the application of electrical voltage provides a facile method to regenerate the MXene membranes	[59]
Ti ₃ C ₂ T _x /poly(vinyl alcohol (PVA)	MB: 97.2 ± 0.8	7.4		
MXene slit membranes (MD simulation)	Monovalent salt ions: 100	400	The material's inherent interaction parameters, hydrophobicity, and shape of the slits were found to affect the desalination performance	[55]

hand, the low flux of Mg²⁺ and Al³⁺ is attributed to the shrinkage interlayer spacing.

The water flux through the pristine MXene (Ti₃C₂T_x) was significantly enhanced from ~ 118 to ~ 420 L (m² h bar)⁻¹

by modifying MXene with Ag nanoparticles (Ag@MXene) [51]. The enhanced water flux after modification is due to a decrease in contact angle and creation of a slit interspacing of 1–4 nm between the MXene nanosheets providing

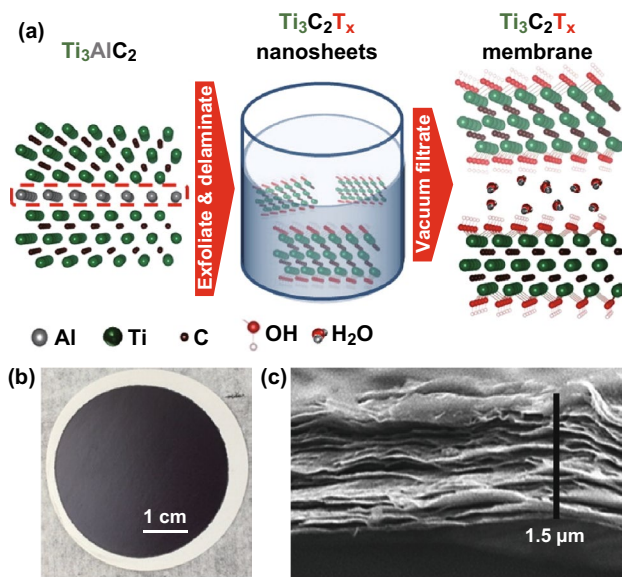


Fig. 2 **a** A schematic of the synthesis of a $\text{Ti}_3\text{C}_2\text{T}_x$ membrane, **b** photograph, and **c** SEM image of cross-sectional of the $\text{Ti}_3\text{C}_2\text{T}_x$ membrane. Reprinted with the permission from Ref. [36]. Copyright © (2015) American Chemical Society

excess nanopores in the Ag@MXene membranes. The Ag@MXene composite membrane also revealed enhanced bactericidal characteristics compared to pristine MXene and polyvinylidene difluoride (PVDF)-based membranes, by exhibiting 99% *E. coli* growth inhibition as shown in Fig. 4. The Ag@MXene composite membrane showed moderate rejection of salts that might be due to their open structure after modification.

The surface charges of the membrane also affect the ion sieving performance, as confirmed by density functional theory calculations [52]. Ions of different charge states behave differently due to the difference in energy barriers for the intercalation, and spacing between the MXene can be expanded or contracted that affects the ion sieving rate. The energy barrier width increased, while the interlayer space decreased, with increasing the charge of the cations, as shown in Fig. 5 [52]. These findings suggest that ion sieving performance of MXene membranes can be enhanced by modifying the surface charges.

Ding et al. [53] prepared MXene nanosheets by etching the Ti_3AlC_2 particles by HF solution to generate $\text{Ti}_3\text{C}_2\text{T}_x$ powder followed by sonication-assisted exfoliation, as shown in Fig. 6. The MXene nanosheets were intercalated by using $\text{Fe}(\text{OH})_3$ colloidal solution that created the expanded nanochannels. The MXene membrane was obtained by a vacuum

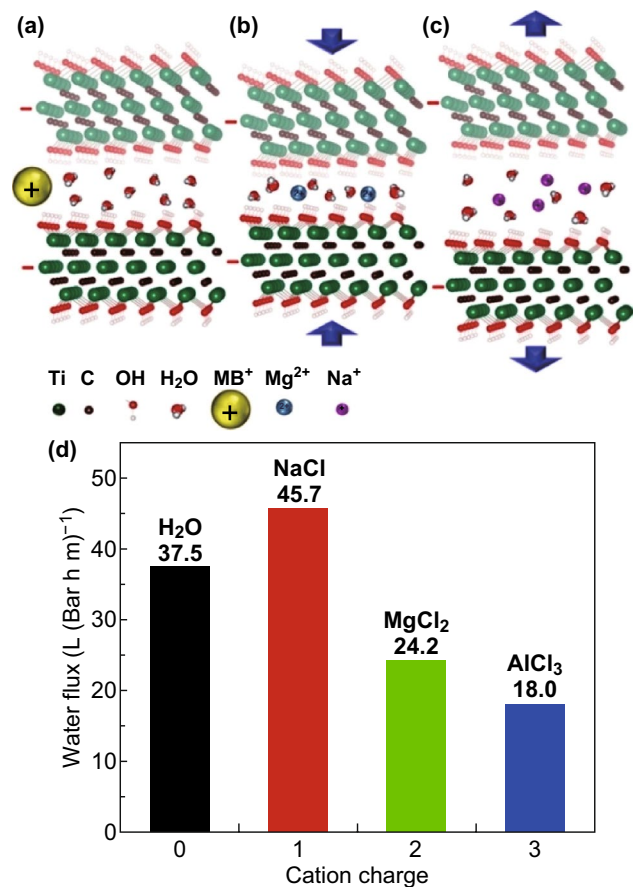


Fig. 3 Schematics of the permeation of cations through a $\text{Ti}_3\text{C}_2\text{T}_x$ membrane and total rejection of large MB^+ . **a** Cations of radii $> 6.4 \text{ \AA}$ cannot penetrate into interlayer spacing. **b** Shrinkage of spacing between $\text{Ti}_3\text{C}_2\text{T}_x$ layers due to the intercalation of smaller multiple-charged cations that result in slower permeation. **c** Expansion of $\text{Ti}_3\text{C}_2\text{T}_x$ interlayer spacing due to the intercalation of small single-charged cations that result in faster flow. **d** The flux of salt solutions and water through the $\text{Ti}_3\text{C}_2\text{T}_x$ membranes versus cation's charge. Reprinted with permission from Ref. [36]. Copyright © (2015) American Chemical Society

filtration process followed by a hydrochloric acid solution (HCl) treatment to eradicate the $\text{Fe}(\text{OH})_3$ nanoparticles.

The highest water flux ($> 1000 \text{ L} (\text{m}^2 \text{ h bar})^{-1}$) was reported by Ding et al. for the MXene membrane supported on anodic aluminum oxide (AAO) substrate [53]. The membrane also demonstrated a promising rejection rate ($> 90\%$) for molecules with sizes larger than 2.5 nm. The enhanced water flux can be ascribed to the surplus nanochannels formed in the MXene membrane after deposition on AAO support.

Membrane permeation performance can be enhanced further by tuning of membrane properties. The interlayer

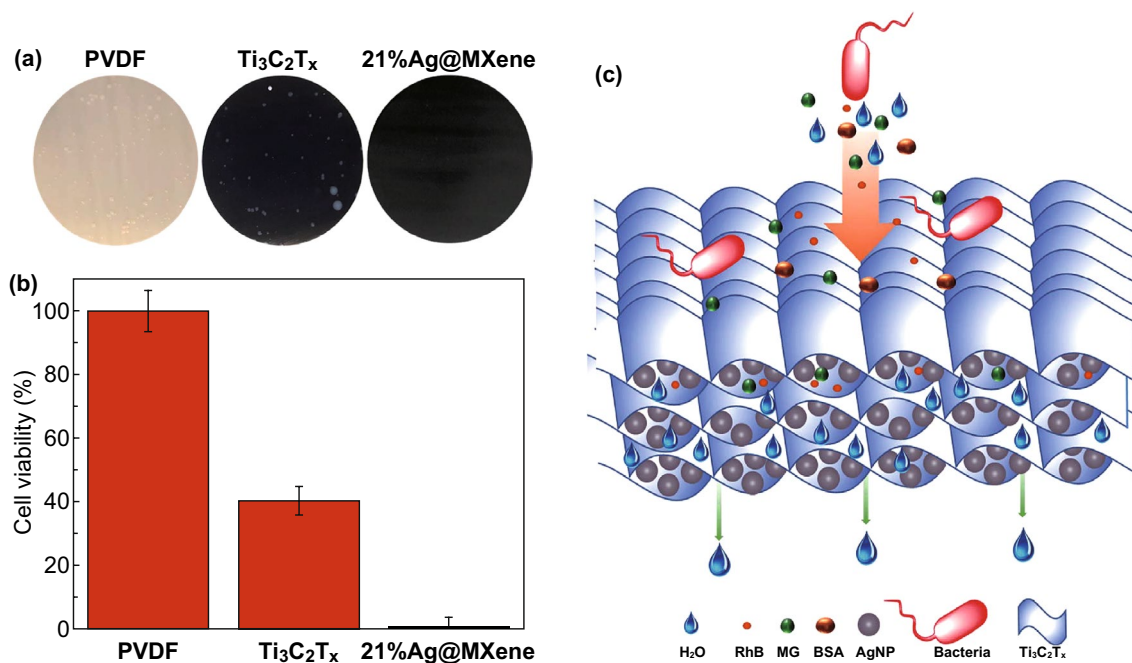


Fig. 4 Antibacterial activity of PVDF (control), MXene ($Ti_3C_2T_x$), and 21% Ag@MXene membranes: **a** photographs of *E. coli* cell growth incubated at 35 °C for 24 h. **b** Cell viability measurements of *E. coli*. **c** Schematic structure and mechanism of rejection of the 21% Ag@MXene composite membrane. Reprinted with permission from Ref. [51]. Copyright © (2019) Royal Society of Chemistry

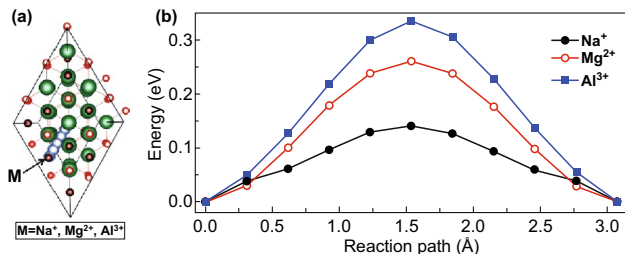


Fig. 5 **a** Considered ion migration pathway and **b** corresponding energy profiles of Na^+ , Mg^{2+} , and Al^{3+} . Reprinted with permission from Ref. [52]. Copyright © (2019) AIP Publishing LLC

spacing between stacked neighboring nanosheets of ultrathin MXene-derived membranes supported on $\alpha-Al_2O_3$ was adjusted by regulating the sintering temperature [54]. MXene membranes were synthesized by depositing the MXene dispersion on the inner surface of the porous ceramic substrate. The prepared membranes were dried and calcinated at different temperatures ranging from 200 to 500 °C in air. The interlayer spacing decreased with an increase in temperature probably due to de-functionalization ($-OH$) occurred within the MXene film at high temperature and moisture loss. At temperature > 400 °C, the oxidation of $Ti_3C_2T_x$ nanosheets into TiO_2 NPs occurs and the ion

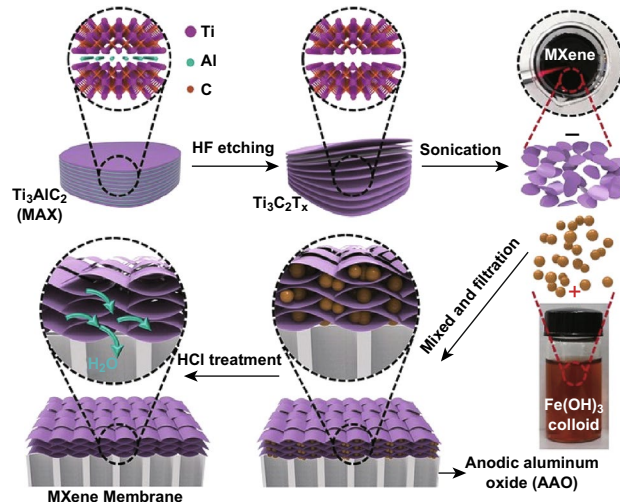


Fig. 6 Schematic of MXene membrane preparation via HF etching and intercalation by using $Fe(OH)_3$ colloidal solution. Reprinted with permission from Ref. [53]. Copyright © 2017 John Wiley & Sons, Inc

retention reduced due to change in filtration mode from interlayer transport pathways to longitudinal nanochannels. The higher retention was obtained for membrane sintered at 400 °C, while the salt rejection of various ions followed the order: $Na_2SO_4 > MgSO_4 > NaCl > MgCl_2$, whereas the water

and salt permeation were greater for membrane calcinated at 200 °C, as depicted in Fig. 7.

The rejection and permeation performance of MXene slit membranes were predicted by molecular dynamics (MD) simulation [55]. The material's inherent interaction parameters, hydrophobicity, and shape of the slits were found to affect the desalination performance. Mixed matrix membrane comprising MXene and P84 copolyimide demonstrated high flux ($268 \text{ L (m}^2 \text{ h)}^{-1}$) at 0.1 MPa and excellent solvent resistance that suggests their potential applications as nanofiltration membranes [56]. The incorporation of the inorganic additive has a positive impact on water permeability and solvent resistance.

Lu et al. [57] synthesized the self-cross-linked MXene membrane through a facile thermal treatment. Self-cross-linking reaction ($-\text{OH}^+ -\text{OH} = -\text{O}^- + \text{H}_2\text{O}$) resulted in the formation of Ti–O–Ti bonds between the MXene nanosheets, as depicted in Fig. 8. The resulting membrane exhibited excellent stability and anti-swelling property in addition to the improved performance of the ion exclusion (98.6% of NaCl) compared to pristine MXene. The stability

of the self-cross-linked MXene membrane compared to polymeric membranes, under acid/base conditions, advocates their promising potential in desalination.

Solvent-resistant polymer– $\text{Ti}_3\text{C}_2\text{T}_x$ nanofiltration membranes exhibited excellent permeation performance for alcohol molecules by providing additional pathways along nanosheet surface using $-\text{OH}$ as an adsorption site [58]. The membrane also demonstrated good solvent resistance and rejection abilities, in addition to improved mechanical and thermal stability. This endorses the probable applications of MXene and polymer composite membranes in desalination.

Ren et al. [59] reported the voltage-gated ions sieving through the nanochanneled $\text{Ti}_3\text{C}_2\text{T}_x$ membrane. The rejection of MgSO_4 and NaCl enhanced by applying a negative electrical potential (-0.6 V) to the $\text{Ti}_3\text{C}_2\text{T}_x$ membrane and inhibited after applying a positive potential due to electrostatic repulsion between the cations and charged MXene layers. The voltage-gated rejection through electronically conductive membranes represents a promising breakthrough approach to improve the elimination of various ions. Figure 9 illustrates orderly stacked 2D nanochannels across the

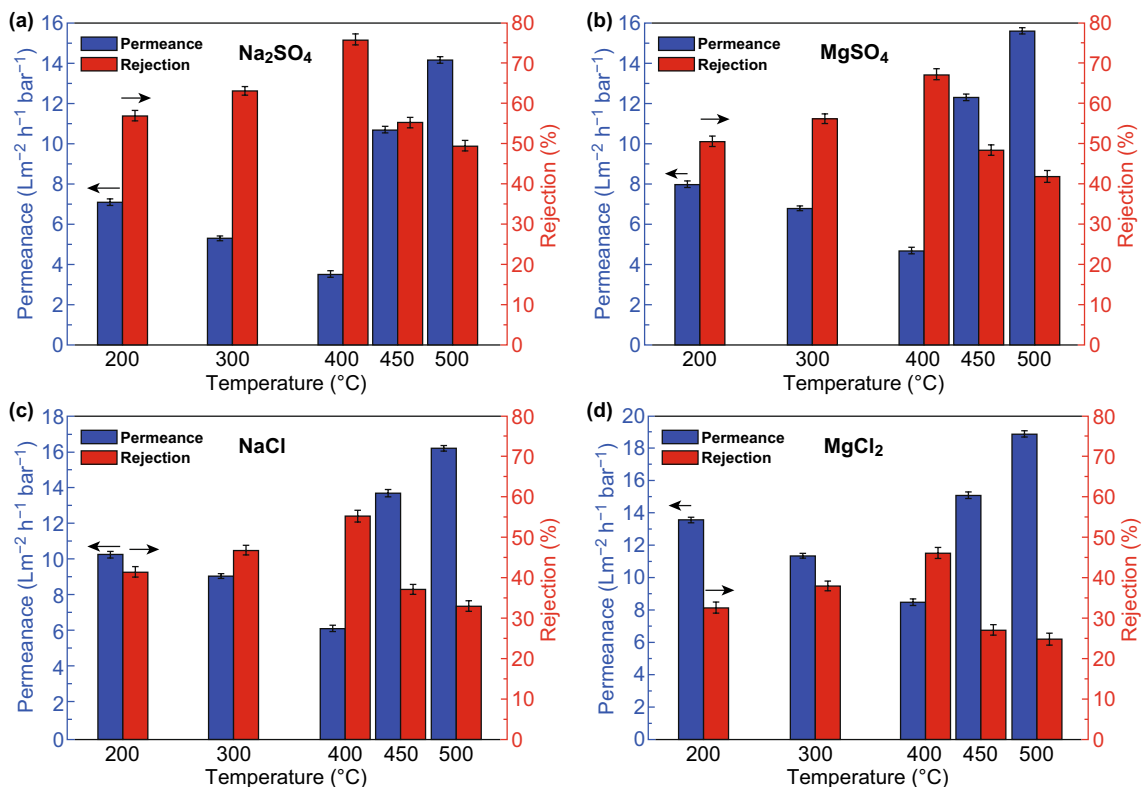


Fig. 7 a–d Rejections and salt permeances of the MXene membranes. Reprinted with permission from Ref. [54]. Copyright © (2019) Elsevier B.V

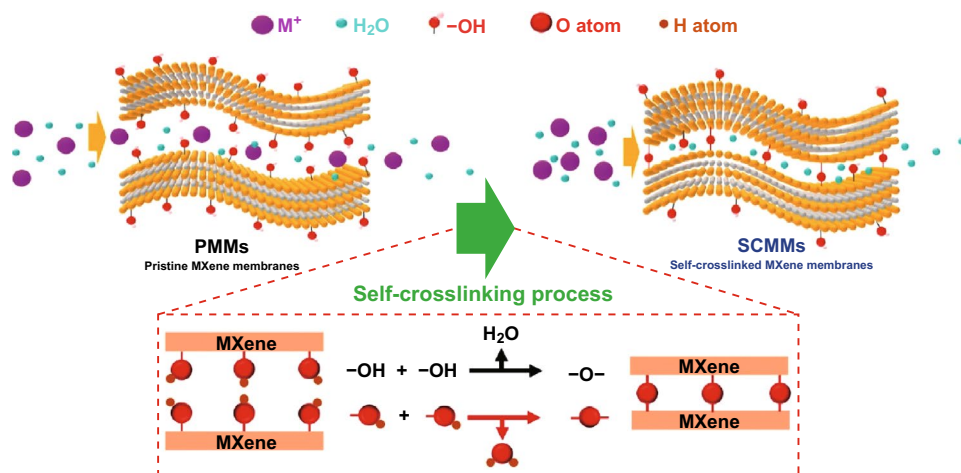


Fig. 8 Self-cross-linking process of the MXene membranes. Reprinted with permission from Ref. [57]. Copyright © (2019) Royal Society of Chemistry

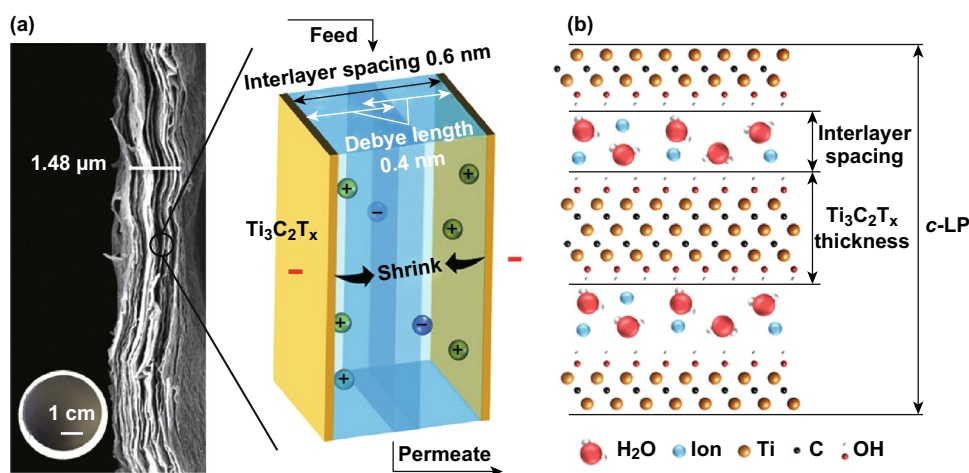


Fig. 9 **a** Cross-sectional SEM image of a $\text{Ti}_3\text{C}_2\text{T}_x$ membrane with a schematic showing the interaction between $\text{Ti}_3\text{C}_2\text{T}_x$ layers and ions within their EDLs when the $\text{Ti}_3\text{C}_2\text{T}_x$ membrane is connected to a negative voltage. **b** Molecular model of $\text{Ti}_3\text{C}_2\text{T}_x$ showing two layers of water with ions between the layers. The c lattice parameter (c -LP) calculated from XRD is two $\text{Ti}_3\text{C}_2\text{T}_x$ flake thicknesses and two interlayer spacings. Reprinted with permission from Ref. [59]. Copyright © (2018) American Chemical Society

structure of a $\text{Ti}_3\text{C}_2\text{T}_x$ membrane and channel (interlayer spacing) between two MXene sheets.

2.2 Capacitive Deionization (CDI)

CDI is an energy-efficient electrochemical process in which anions and cations are separated based on their charge and deposited on positively charged anode and negatively charged cathode, respectively. The selection of electrode materials is critical in the CDI process, and an

ideal electrode must have a high surface area, good electrical conductivity, and high stability. Owing to their superior pseudocapacitive properties, MXenes have emerged as novel electrode materials for CDI applications [60–67]. The MXene-based CDI electrode proved a marvelous adsorption capacity for both cations and anions simultaneously due to their high electrical conductivity, hydrophilicity, and tunable surface [39, 62, 68]. Table 2 summarizes the desalination performance of MXene electrodes in CDI.

Srimuk et al. [39] introduced the MXene-based CDI electrode for the first time by casting Ti_3C_2 onto the porous

Table 2 Desalination performance of MXene electrodes in CDI

Electrode material	Surface area (m ² g ⁻¹)	NaCl concentration (mM)	Cell voltage (V)	Salt removal capacity (mg g ⁻¹)	Remarks	References
Ti ₃ C ₂ MXene	6	5	1.2	13 ± 2	MXene CDI electrodes demonstrated excellent performance in 30 cycles The adsorption of ions onto the electrode occurs via ion intercalation instead of double-layer formation	[39]
Porous Ti ₃ C ₂ T _x MXene	293	10,000 mg L ⁻¹	1.2	45	MXene electrode demonstrated 12 times higher ion adsorption capacity than other carbon-based electrodes and excellent cycling stability (up to 60 cycles)	[62]
Mo _{1.33} C-MXene	1	5/50/600	0.8	5/9/15	Incorporation of carbon nanotubes enhanced the desalination performance of MXene electrode Low energy requirement compared to traditional carbon electrode	[68]
Ar plasma-modified Ti ₃ C ₂ T _x	–	500 mg L ⁻¹	1.4	26.8	Ar plasma modification of MXene nanosheets resulted in the increased interlayer distance between the sheets Electrode showed good regeneration ability and reproducible results	[60]
Porous nitrogen-doped MXene sheets (N-Ti ₃ C ₂ T _x)	368.8	5000 mg L ⁻¹	1.2	43.5 ± 1.7	Nitrogen doping significantly enhances the surface area and desalination performance of MXene	[64]
LiF/HCL-etched Ti ₃ C ₂ T _x MXene	2.1	585	1.2	67.7	The LiF/HCL etching resulted in the increased interlayer spacing of Ti ₃ C ₂ T _x and enhanced desalination capacity	[65]
Preconditioned Ti ₃ C ₂ T _x MXene	–	10	– 1.2 (discharge potential (V))	9.19	Operating conditions such as flow rate, half-cycle length (HCL), and discharge potential affect the desalination performance of electrode	[67]

separator of the CDI cell. MXene CDI electrodes demonstrated excellent performance in 30 cycles with a salt adsorption capacity of 13 ± 2 mg g⁻¹ (1.2 V cell voltage in 5 mM

NaCl saline solution). The adsorption of ions onto the electrode occurs via ion intercalation instead of double-layer formation, as schematically depicted in Fig. 10.

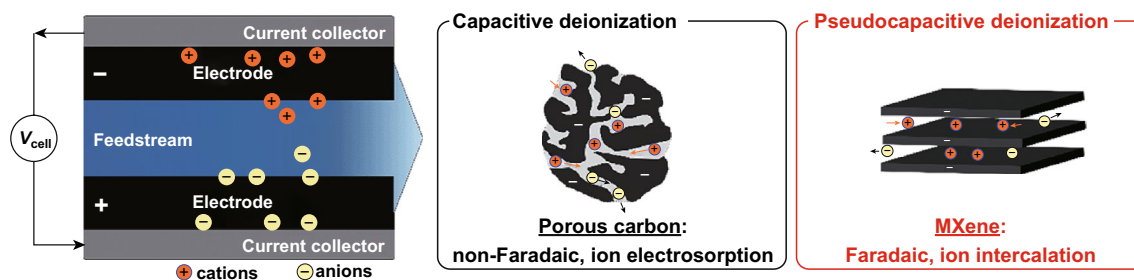


Fig. 10 Concept of electrochemical water desalination by non-faradaic (electrostatic) ion electrosorption at the surface of electrode materials. Reprinted with permission from Ref. [39]. Copyright © (2019) Royal Society of Chemistry

Desalination performance of the MXene electrode was further enhanced by entangling MXene with carbon nanotubes to form a binder-free CDI electrode [68]. The resultant $\text{Mo}_{1.33}\text{C}$ -MXene electrode presented a charge efficiency of $\sim 97\%$ and desalination capacity of 15 mg g^{-1} in 600 mM NaCl . The prepared electrode has the advantage of low energy requirement compared to traditional carbon electrodes. The excellent desalination performance of the electrode in the absence of ion-exchange membranes provides a strong base for its applications in future desalination technology. Incorporation of polymer binders and carbon nanotubes into MXenes results in composite with enhanced electrical conductivity, mechanical strength, and tremendous flexibility that can be exploited for desalination applications [69, 70]. The addition of polymer or nanomaterials also influences the interlayer spacing [70].

Levi et al. [66] demonstrated that two types of cationic adsorption sites (shallow and deep) are present in the interlayer gaps of the $\text{Ti}_3\text{C}_2\text{T}_x$ layers. The swelling of the multilayered $\text{Ti}_3\text{C}_2\text{T}_x$ occurs spontaneously when in contact with the solution at open-circuit potential, and adsorbed cations are electrochemically inserted between partially swollen $\text{Ti}_3\text{C}_2\text{T}_x$ layers. The deep adsorption exists in the particle's interior, while the shallow adsorption sites are present near the edges of the multilayer particles that are water-rich, as depicted in Fig. 11a. Ion accumulation on the deep adsorption is possible by increasing the cathodic current to -0.6 V at slow scan rates after a large number of cycles, and/or by slowly charging and discharging (Fig. 11b). Electrodesorption performance of porous $\text{Ti}_3\text{C}_2\text{T}_x$ electrode in NaCl solution is presented in Fig. 11c, d, while Fig. 11e shows schematics of the CDI process.

Porous $\text{Ti}_3\text{C}_2\text{T}_x$ architectures for CDI applications are prepared by chloroform exfoliation of $\text{Ti}_3\text{C}_2\text{T}_x$ followed by freezing the resultant suspension in liquid nitrogen and vacuum-drying the frozen $\text{Ti}_3\text{C}_2\text{T}_x$ cubes [62]. The process is illustrated schematically in Fig. 12.

Aerogel-like porous MXene electrode material unveiled excellent capacitive deionization performance with 12 times higher ion adsorption capacity than other carbon-based electrodes [62].

The porous MXene electrode exhibited excellent cycling stability (up to 60 cycles) with the reported ion adsorption capacity of 45 mg g^{-1} in a $10,000 \text{ mg L}^{-1}$ salt solution. The ion intercalation into the interlayer space of the MXene also contributes to salt adsorption in addition to capacitive storage. The superior performance of the electrode was attributed to the high electrical conductivity, high surface area, well-defined porous structure, and hydrophilic nature of the $\text{Ti}_3\text{C}_2\text{T}_x$.

The porous $\text{Ti}_3\text{C}_2\text{T}_x$ CDI electrode showed excellent cyclic stability up to 60 cycles (Fig. 11c), and the highest electroadsorption capacitance reaches within $\sim 450 \text{ s}$. The electrode demonstrated good reversibility and was easily regenerated when the applied voltage dropped back to 0 V . The electroadsorption capacities increased with an increase in voltage from 0.8 to 1.2 V , as shown in Fig. 11d.

Doping of MXene sheets with nitrogen yields a porous electrode ($\text{N-Ti}_3\text{C}_2\text{T}_x$) with high surface and promising desalination performance [64]. Nitrogen doping significantly enhances the surface area of MXene to $368.8 \text{ m}^2 \text{ g}^{-1}$ that is the highest value reported in the literature for any MXene-based electrode. $\text{N-Ti}_3\text{C}_2\text{T}_x$ demonstrated an average salt adsorption capacity of $43.5 \pm 1.7 \text{ mg g}^{-1}$ under 1.2 V in 5000 mg L^{-1} NaCl solution. The electrode shows good stability over 24 CDI cycles. The etching process also

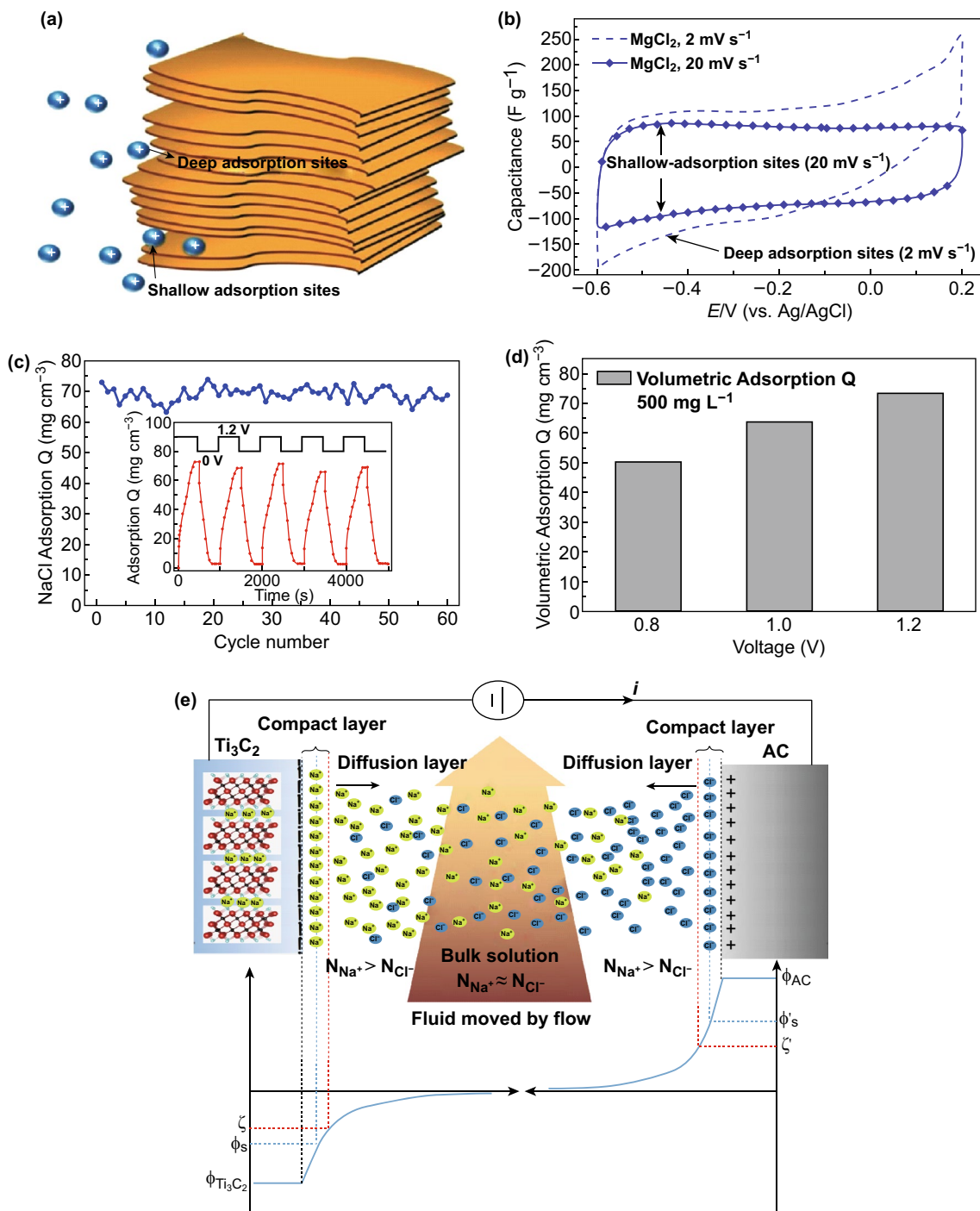


Fig. 11 **a** Schematic illustration of multilayered $Ti_3C_2T_x$ particle containing shallow and deep adsorption sites near the gap opening and in its interior, respectively, **b** Capacitance of $Ti_3C_2T_x$ /carbon black–PTFE laminate in a Swagelok cell measured at scan rates of 2 and 20 mV s^{-1} (dash line and symbols, respectively) in 1 M MgCl_2 related to deep and shallow adsorption sites, respectively. Reprinted with permission from Ref. [66]. Copyright © (2015) John Wiley & Sons, Inc. **c** Electroadsorption and regeneration cycles of porous $Ti_3C_2T_x$ electrode in 500 mg L^{-1} NaCl solution. **d** Electroadsorption capacitance of porous $Ti_3C_2T_x$ at varied voltage in 500 mg L^{-1} NaCl solution. Reprinted with permission from Ref. [62]. Copyright © (2018) Elsevier Inc. **e** Schematics of the CDI process. Reprinted with permission from Ref. [60]. Copyright © (2018) Elsevier B.V

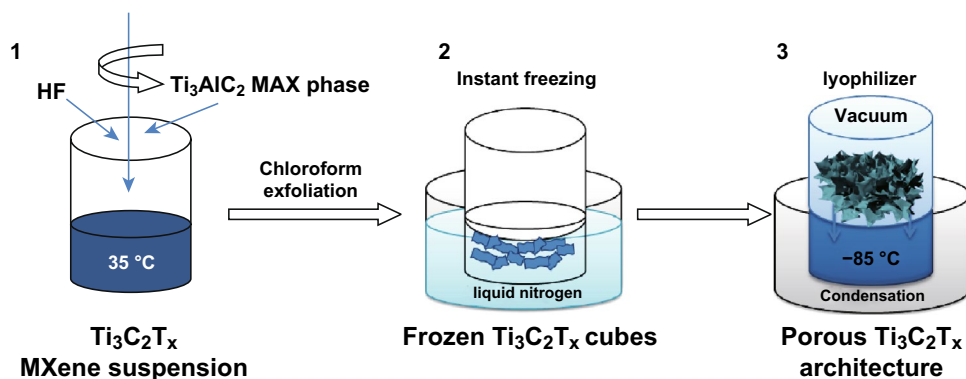


Fig. 12 Synthetic procedure for the porous $\text{Ti}_3\text{C}_2\text{T}_x$ architecture. Reprinted with permission from Ref. [62] Copyright © (2018) Elsevier Inc

influences the desalination characteristics of MXene electrode. Ma et al. [65] employed the LiF/HCL etching method to prepare a freestanding $\text{Ti}_3\text{C}_2\text{T}_x$ MXene electrode without any binder and evaluated its desalination performance. The LiF/HCL etching resulted in the increased interlayer spacing of $\text{Ti}_3\text{C}_2\text{T}_x$ and enhanced desalination capacity. The electrode exhibited a desalination capacity of 68 mg g^{-1} at 1.2 V for NaCl concentration of 585 mg L^{-1} .

Ar plasma modification of MXene nanosheets resulted in the increased interlayer distance between the sheets and hence improved desalination performance [60]. The surface of $\text{Ti}_3\text{C}_2\text{T}_x$ was modified to introduce amorphous carbon and anatase TiO_2 layer using Ar plasma treatment. The desalination performance of the electrode was evaluated using 500 mg L^{-1} NaCl solution in the voltage range of 0.8–1.6 V, as shown in Fig. 11e. The maximum removal capacity of 26.8 mg g^{-1} was obtained at 1.2 V. The Ti_3C_2 -based electrode showed good regeneration ability and reproducible results for several cycles of electrosorption and desorption.

Desalination performance of MXene electrode is influenced by the operating conditions such as flow rate, half-cycle length (HCL), and discharge potential [67]. Agartan et al. [67] reported that salt adsorption rate and capacity increased by 152% at lower discharge potentials and decreased at faster flow rates. Likewise, half-cycle length decreased salt adsorption rate by 54% and capacity by 32%. Preconditioned MXene electrodes exhibited better volumetric performance than activated carbon cloth electrodes owing to their hydrophilicity and high electrochemical activity.

2.3 Solar Desalination

MXenes have superb light-to-heat conversion efficiency that makes them an ideal applicant for application in solar-based desalination [71]. The photothermal water evaporation capability of MXenes is yet another energy-efficient characteristic

Table 3 Solar evaporation performance of MXene membranes

Material	Efficiency (%)	Evaporation rate [$\text{kg (m}^2 \text{ h)}^{-1}$]	Remarks	References
Ti_3C_2 MXene	84	1.373	The MXene, Ti_3C_2 demonstrated 100% light-to-heat conversion efficiency	[71]
Ti_3C_2 MXene	71	1.31	The hydrophobic MXene membrane exhibited excellent solar evaporation potential Not suitable for long-term solar desalination due to poor salt-blocking after an elongated period Extraordinary stability (> 200 h) under actual seawater conditions	[72]
VA-MXA	87	1.46	The hydrophobic upper layer absorbed light and the hydrophilic bottom layer pumped water The high water evaporation rate is attributed to the strong capillary pumping and fast water diffusion through the vertically aligned channels of the VA-MXA	[74]

of these fascinating 2D materials. Table 3 enlists the solar evaporation performance of MXene membranes.

Zhao et al. [72] reported the synthesis and solar desalination potential of the hydrophobic MXene membrane. The delaminated Ti_3C_2 (d- Ti_3C_2) was obtained by HCl/LiF etching from the MAX phase, followed by vacuum deoxidation and ultrasonication, as shown in Fig. 13. The hydrophobic membranes were obtained by surface modification of the d- Ti_3C_2 with trimethoxy(1H,1H,2H,2H-perfluorodecyl) silane (PFDTMS) [72].

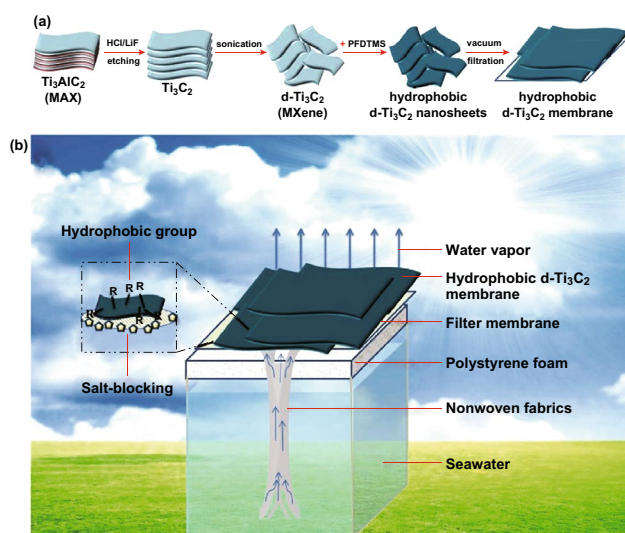


Fig. 13 Schematic illustration of **a** fabrication process of the hydrophobic d- Ti_3C_2 membrane, and **b** the hydrophobic d- Ti_3C_2 membrane-based solar desalination device. Reprinted with permission from Ref. [72]. Copyright © (2019) Royal Society of Chemistry

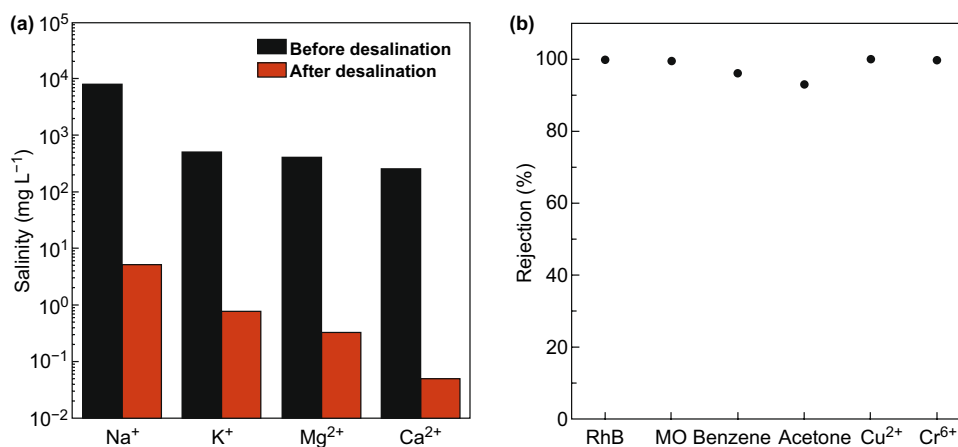


Fig. 14 **a** Measured salinity of four primary ions before and after solar desalination. **b** Organic and heavy metal ion rejection performance. Reprinted with permission from Ref. [72]. Copyright © (2019) Royal Society of Chemistry

The hydrophobic MXene membrane obtained after PFDTMS modification was employed in a solar evaporation device that was self-floated on the seawater. The membrane achieved a solar steam conversion efficiency of 71%, the solar evaporation rate of $1.31 \text{ kg m}^{-2} \text{ h}^{-1}$, and stability under high salinity conditions over 200 h under one sun. The rejection rate for the four primary ions (Ca^{2+} , Mg^{2+} , Mg^{2+} , and Na^{+}) was over 99.5%, while for organic dyes and heavy metals, nearly 100% rejection rate was attained, as shown in Fig. 14. These membranes are not appropriate for long-term solar desalination applications due to poor salt-blocking after an elongated period.

MXene coating improved the antifouling and photo-thermal characteristics of the PVDF (polyvinylidene difluoride) in a solar-assisted direct contact membrane distillation system [73]. MXene-coated membrane demonstrated around 56% reduction in flux decline and a 12% drop in heater energy input per unit volume of distillate. However, MXene-coated membranes exhibited lesser fluxes due to the presence of an additional coating layer.

Zhang et al. [74] reported the desalination performance of vertically aligned Janus MXene aerogel (VA-MXA) with two layers, i.e., hydrophilic (at the bottom) and hydrophobic (at the top). The process of VA-MXA synthesis is presented in Fig. 15. MXene obtained from the Ti_3AlC_2 phase is frozen by liquid nitrogen under Ar protection in a polytetrafluoroethylene (PTFE) mold with a Ti plate. The freezing process yields a black frozen

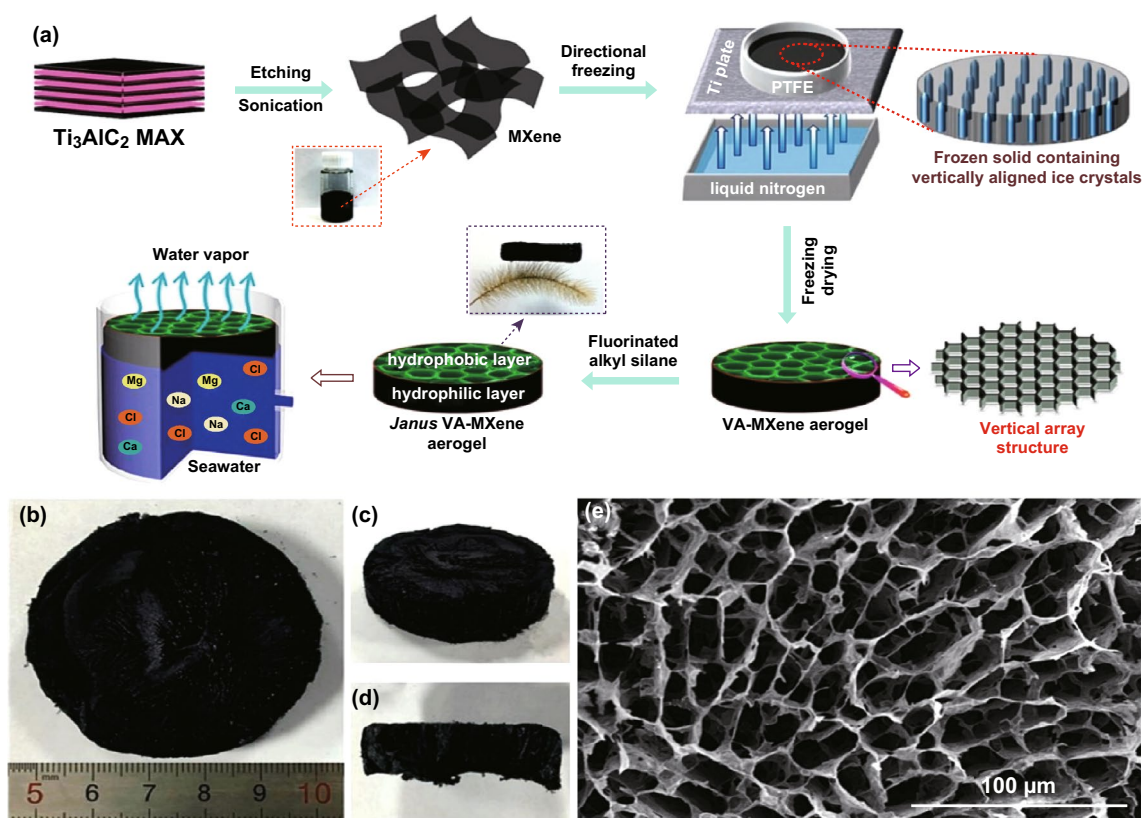


Fig. 15 **a** Fabrication process of a Janus VA-MXA with vertically aligned channels. **b** Digital photograph of the top view of the as-prepared Janus VA-MXA. **c** Photograph of the side view. **d** Photograph of the fracture face. **e** SEM images of the upper layer of prepared Janus VA-MXA. Reprinted with permission from Ref. [74]. Copyright © (2019) American Chemical Society

material consisting of ice crystals surrounded by Ti_3C_2 nanosheets. A vertically aligned framework of the Ti_3C_2 nanosheets is obtained by removing ice crystals via vacuum freeze-drying. The freestanding VA-MXA was placed in a ring-shaped sponge mold, and the hydrophobic layer was formed by floating the sponge on fluorinated alkyl silane under vacuum conditions, followed by drying under Ar environment.

The hydrophilic bottom layer of VA-MXA pumped water and the hydrophobic upper layer absorbed light. The salts crystallized on the hydrophilic bottom layer are quickly dissolved due to continuous pumping of water. The VA-MXA demonstrated an excellent water evaporation rate of $1.46 \text{ kg} (\text{m}^2 \text{ h})^{-1}$ and conversion efficiency of $\sim 87\%$. The high water evaporation rate is attributed to the strong capillary pumping and fast water diffusion through the vertically aligned channels of the VA-MXA.

2.4 Pervaporation Desalination

Pervaporation desalination is a combination of water diffusion through a membrane followed by its evaporation into the vapor phase on the other side of the membrane. MXene/PAN composite and freestanding MXene membranes were prepared by vacuum filtration of the MXene suspension through the polymeric substrate, as shown in Fig. 16 [75]. A specific amount of MXene nanosheets were deposited on PAN substrate to prepare MXene/PAN composite (Fig. 16d–i), while freestanding MXene membranes were prepared via similar approach by using polycarbonate (PC), followed by exfoliation of MXene from substrates after drying for 24 h (Fig. 16a–c). As the amount of MXene nanosheets increases, the thickness of the MXene layer increases and its color varies from light green to dark green.

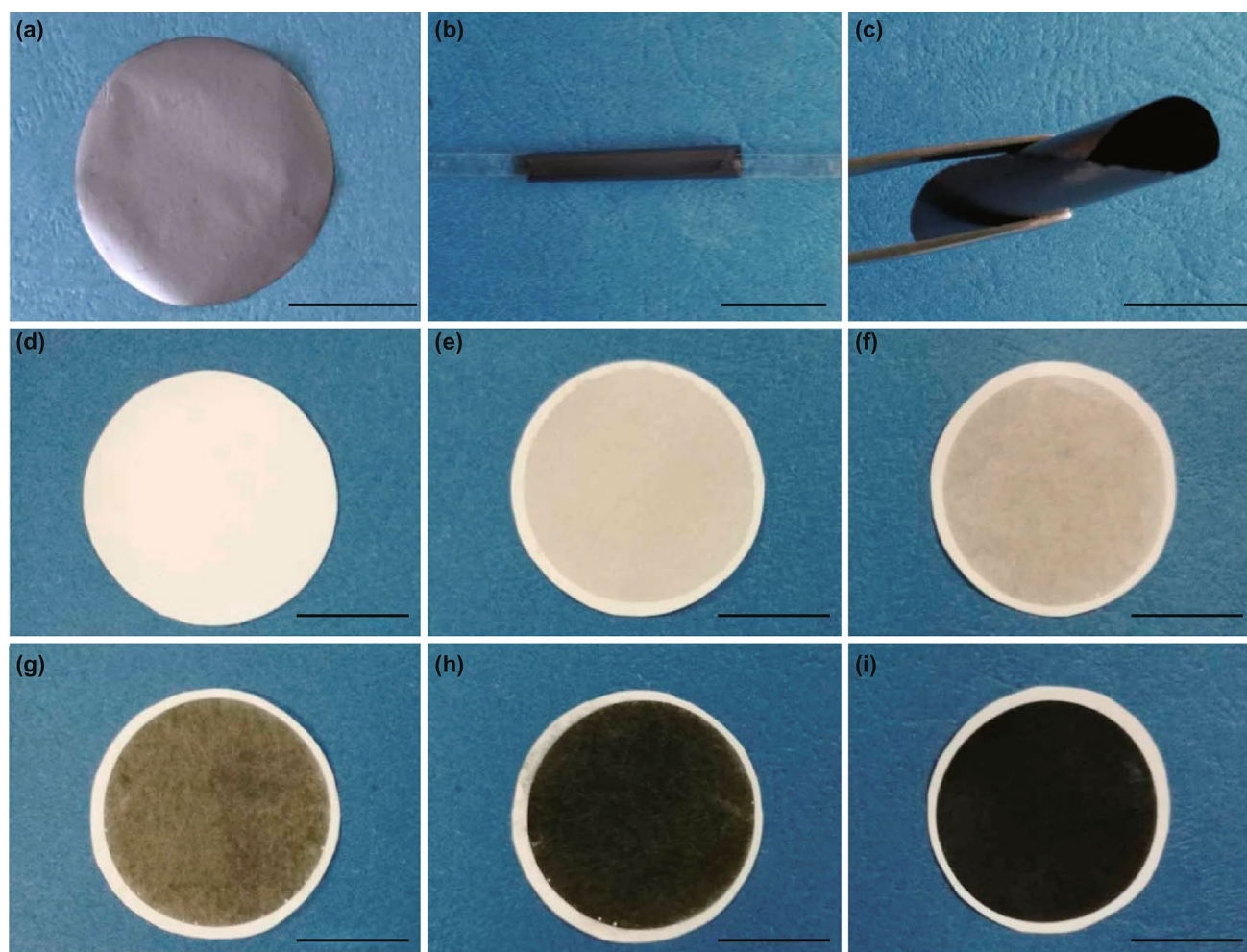


Fig. 16 Digital images of membranes **a** freestanding MXene membrane, **b, c** folded MXene membrane, **d–i** MXene membrane with different deposition amount, i.e., (0, 3.662, 7.325, 18.31, 36.62, 73.25) $\times 10^{-6}$ g cm $^{-2}$. Reprinted with the permission from Ref. [75]. Copyright © (2017) Elsevier B.V

A home-made apparatus was employed to measure the pervaporation desalination performance of the MXene membranes. The membranes consist of stacked atomic-thin MXene nanosheets (~ 60 nm) supported on commercial PAN ultrafiltration membranes exhibiting tremendous potential for pervaporation desalination [75]. The membranes rejected 99.5% salt and exhibited a water flux of $85.4 \text{ L (m}^2 \text{ h)}^{-1}$ at 65°C . The MXene membrane also demonstrated great desalination performance for synthetic seawater compared to the other membranes reported in the literature. One hurdle associated with pervaporation desalination is the intensified use of energy. However, with the utilization of renewable energy or energy from waste sources, a significant improvement in energy efficiency is expected.

3 Challenges and Future Prospects

Although MXenes have emerged as fabulous materials for potential applications in desalination, there are still plentiful challenges and baffling disputes that need to be addressed to fully exploit their remarkable properties [3, 9, 13, 17, 18, 76]. MXenes are mainly synthesized through a top-down route, and very limited literature is available on the synthesis of MXenes using a bottom-up approach [13, 77]. A significant consideration is desired in this research drift to explore the novel bottom-up methods of MXene synthesis with more control of product characteristics.

The MXenes family can be further extended by exploring the synthesis of MXenes from other potential MAX

phases [78]. Furthermore, the same technique for MXene synthesis may be applied to produce more 2D materials from MAX-like phases such as MAB. Another hurdle for researchers to be overcome is the requirement of sub-zero temperatures for the storage of MXenes [79]. It is essential to develop an effective technique for storing MXene solution for a long time without oxidizing.

The traditional method for the synthesis of MXenes using hazardous HF is associated with serious health and environmental concerns. The replacement of HF with green or less toxic chemicals can assure an environment-friendly technique for the synthesis of MXenes. There are some attempts in recent times to substitute HF with less toxic chemicals [8, 80, 81]. However, more attention is required to advance research in this direction. Furthermore, the difficulty in the synthesis of MXenes with uniform and pure surface termination is another obstacle in their practical applications [82].

Another major challenge is the high cost and low yield of MXenes production [17, 18]. Currently, MXenes are mainly produced at the laboratory scale with a small yield. The design of a cost-effective, efficient, and environment-friendly system for the large-scale production of MXenes will be helpful to further advance research in this field and will open a new door of possible applications of MXenes on a commercial scale. It is expected that the cost will be comparatively low for large-scale production.

One more crucial challenge is the need for life cycle analysis and assessment of potential toxic effects of MXenes and MXene-based nanomaterials [18, 83, 84]. Still, studies on the potentially toxic effects of MXenes are limited. With the rapid deployment of MXenes in various applications, it is necessary to fully investigate its lethal effects on the environment, human health, and other organisms. Surface modification of MXenes could be effective in improving its stability, biocompatibility, and recyclability and reducing cytotoxicity. The aggregation of MXenes is also an issue that reduces the adsorption capability and surface area of these 2D materials. The surface chemistry of MXenes and their influence on the removal of pollutants must be further explored to fully understand the removal mechanisms.

Until now, $Ti_3C_2T_x$ is extensively employed in desalination and water treatment, and it is essential to develop a new MXene structure and discover other environmental

remediation applications of various MXenes. Moreover, several theoretical studies such as DFT predicted superior characteristics of MXenes in desalination and environmental remediation applications [17, 85–87]. Proper experimentation and development of an efficient system are required to confirm the results of these theoretical studies [88–90]. There is no suspicion that commercial MXene-based product will be introduced in the market soon and MXenes will discover their role in the future direction of desalination technology. Based on the current promising results, it can be securely foreseen that MXenes could be the next-generation materials for water treatment and desalination.

4 Conclusion

MXenes and MXene-based nanomaterials have offered tremendous advantages, and they have emerged as ideal entrants for future desalination technology. Despite copious hurdles that need to be addressed, based on the promising results from the current research, a remarkable development in the synthesis techniques and applications of these exceptional nanomaterials is anticipated in the near future. For MXenes to be a forerunner in desalination, further research is vital to overawe the existing hurdles. There is no suspicion that MXenes has assured an era of the next-generation 2D nanomaterials and will have a bright future in water purification and environmental remediation.

Acknowledgements The author gratefully acknowledges the support provided by King Fahd University of Petroleum and Minerals (KFUPM), Saudi Arabia. The author would also like to acknowledge the support of the Center for Environment and Water (CEW), Research Institute, at KFUPM.

Open Access This article is licensed under a Creative Commons Attribution 4.0 International License, which permits use, sharing, adaptation, distribution and reproduction in any medium or format, as long as you give appropriate credit to the original author(s) and the source, provide a link to the Creative Commons licence, and indicate if changes were made. The images or other third party material in this article are included in the article's Creative Commons licence, unless indicated otherwise in a credit line to the material. If material is not included in the article's Creative Commons licence and your intended use is not permitted by statutory regulation or exceeds the permitted use, you will need to obtain permission directly from the copyright holder. To view a copy of this licence, visit <http://creativecommons.org/licenses/by/4.0/>.

References

1. M. Naguib, M. Kurtoglu, V. Presser, J. Lu, J. Niu et al., Two-dimensional nanocrystals produced by exfoliation of Ti_3AlC_2 . *Adv. Mater.* **23**, 4248–4253 (2011). <https://doi.org/10.1002/adma.201102306>
2. M. Naguib, O. Mashtalir, J. Carle, V. Presser, J. Lu, L. Hultman, Y. Gogotsi, M.W. Barsoum, Two-dimensional transition metal carbides. *ACS Nano* **6**, 1322–1331 (2012). <https://doi.org/10.1021/nn204153h>
3. M. Naguib, V.N. Mochalin, M.W. Barsoum, Y. Gogotsi, 25th anniversary article: MXenes: a new family of two-dimensional materials. *Adv. Mater.* **26**, 992–1005 (2014). <https://doi.org/10.1002/adma.201304138>
4. N.R. Hemanth, B. Kandasubramanian, Recent advances in 2D MXenes for enhanced cation intercalation in energy harvesting applications: a review. *Chem. Eng. J.* (2019). <https://doi.org/10.1016/j.cej.2019.123678>
5. B. Anasori, Y. Xie, M. Beidaghi, J. Lu, B.C. Hosler et al., Two-dimensional, ordered, double transition metals carbides (MXenes). *ACS Nano* **9**, 9507–9516 (2015). <https://doi.org/10.1021/acs.nano.5b03591>
6. B. Anasori, M.R. Lukatskaya, Y. Gogotsi, 2D metal carbides and nitrides (MXenes) for energy storage. *Nat. Rev. Mater.* **2**, 16098 (2017). <https://doi.org/10.1038/natrevmats.2016.98>
7. W. Sun, S.A. Shah, Y. Chen, Z. Tan, H. Gao, T. Habib, M. Radovic, M.J. Green, Electrochemical etching of Ti_2AlC to Ti_2CT_x (MXene) in low-concentration hydrochloric acid solution. *J. Mater. Chem. A* **5**, 21663–21668 (2017). <https://doi.org/10.1039/C7TA05574A>
8. S. Yang, P. Zhang, F. Wang, A.G. Ricciardulli, M.R. Lohe, P.W.M. Blom, X. Feng, Fluoride-free synthesis of two-dimensional titanium carbide (MXene) using a binary aqueous system. *Angew. Chem. Int. Ed.* **130**, 15717–15721 (2018). <https://doi.org/10.1002/ange.201809662>
9. J.-C. Lei, X. Zhang, Z. Zhou, Recent advances in MXene: preparation, properties, and applications. *Front. Phys.* **10**, 276–286 (2015). <https://doi.org/10.1007/s11467-015-0493-x>
10. O. Mashtalir, M. Naguib, V.N. Mochalin, Y. Dall’Agnese, M. Heon, M.W. Barsoum, Y. Gogotsi, Intercalation and delamination of layered carbides and carbonitrides. *Nat. Commun.* **4**, 1716 (2013). <https://doi.org/10.1038/ncomms2664>
11. M. Magnuson, M. Mattesini, Chemical bonding and electronic-structure in MAX phases as viewed by X-ray spectroscopy and density functional theory. *Thin Solid Films* **621**, 108–130 (2017). <https://doi.org/10.1016/j.tsf.2016.11.005>
12. M.W. Barsoum, T. El-Raghy, Synthesis and characterization of a remarkable ceramic: Ti_3SiC_2 . *J. Am. Ceram. Soc.* **79**, 1953–1956 (1996). <https://doi.org/10.1111/j.1151-2916.1996.tb08018.x>
13. B. Anasori, Y. Gogotsi, *2D metal carbides and nitrides (MXenes), structure, properties and applications* (Springer, Berlin, 2019). <https://doi.org/10.1007/978-3-030-19026-2>
14. A. Szuplewska, D. Kulpińska, A. Dybko, M. Chudy, A.M. Jastrzębska, A. Olszyna, Z. Brzózka, Future applications of MXenes in biotechnology, nanomedicine, and sensors. *Trends Biotechnol.* (2019). <https://doi.org/10.1016/j.tibtech.2019.09.001>
15. M.W. Barsoum, The $M_{N+1}AX_N$ phases: a new class of solids—thermodynamically stable nanolaminates. *Prog. Solid State Chem.* **28**, 201–281 (2000). [https://doi.org/10.1016/S0079-6786\(00\)00006-6](https://doi.org/10.1016/S0079-6786(00)00006-6)
16. Y.-J. Zhang, J.-H. Lan, L. Wang, Q.-Y. Wu, C.-Z. Wang, T. Bo, Z.-F. Chai, W.-Q. Shi, Adsorption of uranyl species on hydroxylated titanium carbide nanosheet: a first-principles study. *J. Hazard. Mater.* **308**, 402–410 (2016). <https://doi.org/10.1016/j.jhazmat.2016.01.053>
17. R.M. Ronchi, J.T. Arantes, S.F. Santos, Synthesis, structure, properties and applications of MXenes: current status and perspectives. *Ceram. Int.* **45**, 18167–18188 (2019). <https://doi.org/10.1016/j.ceramint.2019.06.114>
18. K. Rasool, R.P. Pandey, P.A. Rasheed, S. Buczek, Y. Gogotsi, K.A. Mahmoud, Water treatment and environmental remediation applications of two-dimensional metal carbides (MXenes). *Mater. Today* **30**, 80–102 (2019). <https://doi.org/10.1016/j.mattod.2019.05.017>
19. K. Hantanasirisakul, M. Alhabeb, A. Lipatov, K. Maleski, B. Anasori et al., Effects of synthesis and processing on optoelectronic properties of titanium carbonitride MXene. *Chem. Mater.* **31**, 2941–2951 (2019). <https://doi.org/10.1021/acs.chemmater.9b00401>
20. M. Khazaei, M. Arai, T. Sasaki, C.-Y. Chung, N.S. Venkataramanan, M. Estili, Y. Sakka, Y. Kawazoe, Novel electronic and magnetic properties of two-dimensional transition metal carbides and nitrides. *Adv. Funct. Mater.* **23**, 2185–2192 (2013). <https://doi.org/10.1002/adfm.201202502>
21. M. Khazaei, M. Arai, T. Sasaki, M. Estili, Y. Sakka, Two-dimensional molybdenum carbides: potential thermoelectric materials of the MXene family. *Phys. Chem. Chem. Phys.* **16**, 7841–7849 (2014). <https://doi.org/10.1039/C4CP00467A>
22. X. Liang, Y. Rangom, C.Y. Kwok, Q. Pang, L.F. Nazar, Interwoven MXene nanosheet/carbon-nanotube composites as Li–S cathode hosts. *Adv. Mater.* **29**, 1603040 (2017). <https://doi.org/10.1002/adma.201603040>
23. M. Naguib, R.A. Adams, Y. Zhao, D. Zemlyanov, A. Varma, J. Nanda, V.G. Pol, Electrochemical performance of MXenes as K-ion battery anodes. *Chem. Commun.* **53**, 6883–6886 (2017). <https://doi.org/10.1039/C7CC02026K>
24. P. Urbankowski, B. Anasori, K. Hantanasirisakul, L. Yang, L. Zhang et al., 2D molybdenum and vanadium nitrides synthesized by ammoniation of 2D transition metal carbides (MXenes). *Nanoscale* **9**, 17722–17730 (2017). <https://doi.org/10.1039/C7NR06721F>
25. K. Huang, Z. Li, J. Lin, G. Han, P. Huang, Two-dimensional transition metal carbides and nitrides (MXenes) for biomedical applications. *Chem. Soc. Rev.* **47**, 5109–5124 (2018). <https://doi.org/10.1039/C7CS00838D>
26. V.M.H. Ng, H. Huang, K. Zhou, P.S. Lee, W. Que, J.Z. Xu, L.B. Kong, Recent progress in layered transition metal carbides and/or nitrides (MXenes) and their composites: synthesis and applications. *J. Mater. Chem. A* **5**, 3039–3068 (2017). <https://doi.org/10.1039/C6TA06772G>



27. X. Zhan, C. Si, J. Zhou, Z. Sun, MXene and MXene-based composites: synthesis, properties and environment-related applications. *Nanoscale Horiz.* **5**, 235–258 (2020). <https://doi.org/10.1039/C9NH00571D>
28. J. Zhu, E. Ha, G. Zhao, Y. Zhou, D. Huang et al., Recent advance in MXenes: a promising 2D material for catalysis, sensor and chemical adsorption. *Coord. Chem. Rev.* **352**, 306–327 (2017). <https://doi.org/10.1016/j.ccr.2017.09.012>
29. S. Zhang, S. Liao, F. Qi, R. Liu, T. Xiao et al., Direct deposition of two-dimensional MXene nanosheets on commercially available filter for fast and efficient dye removal. *J. Hazard. Mater.* **384**, 121367 (2019). <https://doi.org/10.1016/j.jhazmat.2019.121367>
30. K. Li, X. Wang, S. Li, P. Urbankowski, J. Li, Y. Xu, Y. Gogotsi, An ultrafast conducting polymer@MXene positive electrode with high volumetric capacitance for advanced asymmetric supercapacitors. *Small* **16**, 1906851 (2019). <https://doi.org/10.1002/sml.201906851>
31. Q. Zhang, J. Teng, G. Zou, Q. Peng, Q. Du, T. Jiao, J. Xiang, Efficient phosphate sequestration for water purification by unique sandwich-like MXene/magnetic iron oxide nanocomposites. *Nanoscale* **8**, 7085–7093 (2016). <https://doi.org/10.1039/C5NR09303A>
32. L. Cheng, X. Li, H. Zhang, Q. Xiang, Two-dimensional transition metal MXene-based photocatalysts for solar fuel generation. *J. Phys. Chem. Lett.* **10**, 3488–3494 (2019). <https://doi.org/10.1021/acs.jpcclett.9b00736>
33. P. Zhang, L. Wang, L.-Y. Yuan, J.-H. Lan, Z.-F. Chai, W.-Q. Shi, Sorption of Eu(III) on MXene-derived titanate structures: the effect of nano-confined space. *Chem. Eng. J.* **370**, 1200–1209 (2019). <https://doi.org/10.1016/j.cej.2019.03.286>
34. Z. Guo, J. Zhou, L. Zhu, Z. Sun, MXene: a promising photocatalyst for water splitting. *J. Mater. Chem. A* **4**, 11446–11452 (2016). <https://doi.org/10.1039/C6TA04414J>
35. H. Jiang, Z. Wang, Q. Yang, L. Tan, L. Dong, M. Dong, Ultrathin $\text{Ti}_3\text{C}_2\text{T}_x$ (MXene) nanosheets wrapped NiSe_2 octahedral crystal for enhanced supercapacitor performance and synergetic electrocatalytic water splitting. *Nano-Micro Lett.* **11**, 31 (2019). <https://doi.org/10.1007/s40820-019-0309-6>
36. C.E. Ren, K.B. Hatzell, M. Alhabeab, Z. Ling, K.A. Mahmoud, Y. Gogotsi, Charge- and size-selective ion sieving through $\text{Ti}_3\text{C}_2\text{T}_x$ MXene membranes. *J. Phys. Chem. Lett.* **6**, 4026–4031 (2015). <https://doi.org/10.1021/acs.jpcclett.5b01895>
37. A. Shahzad, K. Rasool, W. Miran, M. Nawaz, J. Jang, K.A. Mahmoud, D.S. Lee, Two-dimensional $\text{Ti}_3\text{C}_2\text{T}_x$ MXene nanosheets for efficient copper removal from water. *ACS Sustain. Chem. Eng.* **5**, 11481–11488 (2017). <https://doi.org/10.1021/acssuschemeng.7b02695>
38. Y. Ying, Y. Liu, X. Wang, Y. Mao, W. Cao, P. Hu, X. Peng, Two-dimensional titanium carbide for efficiently reductive removal of highly toxic chromium(VI) from water. *ACS Appl. Mater. Interfaces.* **7**, 1795–1803 (2015). <https://doi.org/10.1021/am5074722>
39. P. Srimuk, F. Kaasik, B. Krüner, A. Tolosa, S. Fleischmann et al., MXene as a novel intercalation-type pseudocapacitive cathode and anode for capacitive deionization. *J. Mater. Chem. A* **4**, 18265–18271 (2016). <https://doi.org/10.1039/C6TA07833H>
40. M.A. Iqbal, S.I. Ali, F. Amin, A. Tariq, M.Z. Iqbal, S. Rizwan, La- and Mn-codoped Bismuth Ferrite/ Ti_3C_2 MXene composites for efficient photocatalytic degradation of Congo Red dye. *ACS Omega* **4**, 8661–8668 (2019). <https://doi.org/10.1021/acsomega.9b00493>
41. P. Zhang, M. Xiang, H. Liu, C. Yang, S. Deng, Novel two-dimensional magnetic titanium carbide for methylene blue removal over a wide pH range: insight into removal performance and mechanism. *ACS Appl. Mater. Interfaces.* **11**, 24027–24036 (2019). <https://doi.org/10.1021/acsaami.9b04222>
42. Q. Huang, Y. Liu, T. Cai, X. Xia, Simultaneous removal of heavy metal ions and organic pollutant by $\text{BiOBr}/\text{Ti}_3\text{C}_2$ nanocomposite. *J. Photochem. Photobiol. A Chem.* **375**, 201–208 (2019). <https://doi.org/10.1016/j.jphotochem.2019.02.026>
43. I. Persson, J. Halim, H. Lind, T.W. Hansen, J.B. Wagner et al., 2D transition metal carbides (MXenes) for carbon capture. *Adv. Mater.* **31**, 1805472 (2019). <https://doi.org/10.1002/adma.201805472>
44. T. Liu, X. Liu, N. Graham, W. Yu, K. Sun, Two-dimensional MXene incorporated graphene oxide composite membrane with enhanced water purification performance. *J. Memb. Sci.* **593**, 117431 (2020). <https://doi.org/10.1016/j.memsci.2019.117431>
45. B.-M. Jun, S. Kim, J. Heo, C.M. Park, N. Her et al., Review of MXenes as new nanomaterials for energy storage/delivery and selected environmental applications. *Nano Res.* **12**, 471–487 (2019). <https://doi.org/10.1007/s12274-018-2225-3>
46. J. Saththasivam, K. Wang, W. Yiming, Z. Liu, K.A. Mahmoud, A flexible $\text{Ti}_3\text{C}_2\text{T}_x$ (MXene)/paper membrane for efficient oil/water separation. *RSC Adv.* **9**, 16296–16304 (2019). <https://doi.org/10.1039/C9RA02129A>
47. X.-J. Zha, X. Zhao, J.-H. Pu, L.-S. Tang, K. Ke et al., Flexible anti-biofouling MXene/cellulose fibrous membrane for sustainable solar-driven water purification. *ACS Appl. Mater. Interfaces.* **11**, 36589–36597 (2019). <https://doi.org/10.1021/acsaami.9b10606>
48. Z. Xie, Y.-P. Peng, L. Yu, C. Xing, M. Qiu, J. Hu, H. Zhang, Solar-inspired water purification based on emerging two-dimensional materials: status and challenges. *Sol. RRL* (2019). <https://doi.org/10.1002/solr.201900400>
49. M. Ghidui, M.R. Lukatskaya, M.-Q. Zhao, Y. Gogotsi, M.W. Barsoum, Conductive two-dimensional titanium carbide ‘clay’ with high volumetric capacitance. *Nature* **516**, 78–81 (2014). <https://doi.org/10.1038/nature13970>
50. Y. Zhou, F. Wang, H. Wang, Y. Deng, C. Song, Z. Li, Ling, Water permeability in MXene membranes: process matters. *Chin. Chem. Lett.* (2019). <https://doi.org/10.1016/j.ccllet.2019.10.037>
51. R.P. Pandey, K. Rasool, V.E. Madhavan, B. Aïssa, Y. Gogotsi, K.A. Mahmoud, Ultrahigh-flux and fouling-resistant membranes based on layered silver/MXene ($\text{Ti}_3\text{C}_2\text{T}_x$) nanosheets. *J. Mater. Chem. A* **6**, 3522–3533 (2018). <https://doi.org/10.1039/C7TA10888E>

52. G.R. Berdiyrov, M.E. Madjet, K.A. Mahmoud, Ionic sieving through $\text{Ti}_3\text{C}_2(\text{OH})_2$ MXene: first-principles calculations. *Appl. Phys. Lett.* **108**, 113110 (2016). <https://doi.org/10.1063/1.4944393>
53. L. Ding, Y. Wei, Y. Wang, H. Chen, J. Caro, H. Wang, A two-dimensional lamellar membrane: MXene nanosheet stacks. *Angew. Chem. Int. Ed.* **56**, 1825–1829 (2017). <https://doi.org/10.1002/anie.201609306>
54. Y. Sun, S. Li, Y. Zhuang, G. Liu, W. Xing, W. Jing, Adjustable interlayer spacing of ultrathin MXene-derived membranes for ion rejection. *J. Memb. Sci.* **591**, 117350 (2019). <https://doi.org/10.1016/j.memsci.2019.117350>
55. E.Y.M. Ang, T.Y. Ng, J. Yeo, R. Lin, Z. Liu, K.R. Geethalakshmi, Investigations on different two-dimensional materials as slit membranes for enhanced desalination. *J. Memb. Sci.* (2019). <https://doi.org/10.1016/j.memsci.2019.117653>
56. R. Han, Y. Xie, X. Ma, Crosslinked P84 copolyimide/MXene mixed matrix membrane with excellent solvent resistance and permselectivity. *Chin. J. Chem. Eng.* **27**, 877–883 (2019). <https://doi.org/10.1016/j.cjche.2018.10.005>
57. Z. Lu, Y. Wei, J. Deng, L. Ding, Z.-K. Li, H. Wang, Self-crosslinked MXene ($\text{Ti}_3\text{C}_2\text{T}_x$) membranes with good anti-swelling property for monovalent metal ion exclusion. *ACS Nano* **13**, 10535–10544 (2019). <https://doi.org/10.1021/acsnano.9b04612>
58. X. Wu, L. Hao, J. Zhang, X. Zhang, J. Wang, J. Liu, Polymer- $\text{Ti}_3\text{C}_2\text{T}_x$ composite membranes to overcome the trade-off in solvent resistant nanofiltration for alcohol-based system. *J. Memb. Sci.* **515**, 175–188 (2016). <https://doi.org/10.1016/j.memsci.2016.05.048>
59. C.E. Ren, M. Alhabeab, B.W. Byles, M.-Q. Zhao, B. Anasori, E. Pomerantseva, K.A. Mahmoud, Y. Gogotsi, Voltage-gated ions sieving through 2D MXene $\text{Ti}_3\text{C}_2\text{T}_x$ membranes. *ACS Appl. Nano Mater.* **1**, 3644–3652 (2018). <https://doi.org/10.1021/acsnano.8b00762>
60. L. Guo, X. Wang, Z.Y. Leong, R. Mo, L. Sun, H.Y. Yang, Ar plasma modification of 2D MXene $\text{Ti}_3\text{C}_2\text{T}_x$ nanosheets for efficient capacitive desalination. *FlatChem* **8**, 17–24 (2018). <https://doi.org/10.1016/j.flatc.2018.01.001>
61. R. Malik, Maxing out water desalination with MXenes. *Joule* **2**, 591–593 (2018). <https://doi.org/10.1016/j.joule.2018.04.001>
62. W. Bao, X. Tang, X. Guo, S. Choi, C. Wang, Y. Gogotsi, G. Wang, Porous cryo-dried MXene for efficient capacitive deionization. *Joule* **2**, 778–787 (2018). <https://doi.org/10.1016/j.joule.2018.02.018>
63. M.E. Suss, V. Presser, Water desalination with energy storage electrode materials. *Joule* **2**, 10–15 (2018). <https://doi.org/10.1016/j.joule.2017.12.010>
64. A. Amiri, Y. Chen, C.B. Teng, M. Naraghi, Porous nitrogen-doped MXene-based electrodes for capacitive deionization. *Energy Storage Mater.* **25**, 731–739 (2020). <https://doi.org/10.1016/j.ensm.2019.09.013>
65. J. Ma, Y. Cheng, L. Wang, X. Dai, F. Yu, Free-standing $\text{Ti}_3\text{C}_2\text{T}_x$ MXene film as binder-free electrode in capacitive deionization with an ultrahigh desalination capacity. *Chem. Eng. J.* (2019). <https://doi.org/10.1016/j.cej.2019.123329>
66. M.D. Levi, M.R. Lukatskaya, S. Sigalov, M. Beidaghi, N. Shpigel et al., Solving the capacitive paradox of 2D MXene using electrochemical quartz-crystal admittance and in situ electronic conductance measurements. *Adv. Energy Mater.* **5**, 1400815 (2015). <https://doi.org/10.1002/aenm.201400815>
67. L. Agartan, K. Hantanasirisakul, S. Buczek, B. Akuzum, K.A. Mahmoud, B. Anasori, Y. Gogotsi, E.C. Kumbur, Influence of operating conditions on the desalination performance of a symmetric pre-conditioned $\text{Ti}_3\text{C}_2\text{T}_x$ -MXene membrane capacitive deionization system. *Desalination* **477**, 114267 (2020). <https://doi.org/10.1016/j.desal.2019.114267>
68. P. Srimuk, J. Halim, J. Lee, Q. Tao, J. Rosen, V. Presser, Two-dimensional molybdenum carbide (MXene) with divacancy ordering for brackish and seawater desalination via cation and anion intercalation. *ACS Sustain. Chem. Eng.* **6**, 3739–3747 (2018). <https://doi.org/10.1021/acssuschemeng.7b04095>
69. Z. Ling, C.E. Ren, M.-Q. Zhao, J. Yang, J.M. Giammarco, J. Qiu, M.W. Barsoum, Y. Gogotsi, Flexible and conductive MXene films and nanocomposites with high capacitance. *Proc. Natl. Acad. Sci.* **111**, 16676–16681 (2014). <https://doi.org/10.1073/pnas.1414215111>
70. M.-Q. Zhao, C.E. Ren, Z. Ling, M.R. Lukatskaya, C. Zhang, K.L. Van Aken, M.W. Barsoum, Y. Gogotsi, Flexible MXene/carbon nanotube composite paper with high volumetric capacitance. *Adv. Mater.* **27**, 339–345 (2015). <https://doi.org/10.1002/adma.201404140>
71. R. Li, L. Zhang, L. Shi, P. Wang, MXene Ti_3C_2 : an effective 2D light-to-heat conversion material. *ACS Nano* **11**, 3752–3759 (2017). <https://doi.org/10.1021/acsnano.6b08415>
72. J. Zhao, Y. Yang, C. Yang, Y. Tian, Y. Han, J. Liu, X. Yin, W. Que, A hydrophobic surface enabled salt-blocking 2D Ti_3C_2 MXene membrane for efficient and stable solar desalination. *J. Mater. Chem. A* **6**, 16196–16204 (2018). <https://doi.org/10.1039/C8TA05569F>
73. Y.Z. Tan, H. Wang, L. Han, M.B. Tanis-Kanbur, M.V. Prannav, J.W. Chew, Photothermal-enhanced and fouling-resistant membrane for solar-assisted membrane distillation. *J. Memb. Sci.* **565**, 254–265 (2018). <https://doi.org/10.1016/j.memsci.2018.08.032>
74. Q. Zhang, G. Yi, Z. Fu, H. Yu, S. Chen, X. Quan, Vertically aligned janus MXene-based aerogels for solar desalination with high efficiency and salt resistance. *ACS Nano* **13**, 13196–13207 (2019). <https://doi.org/10.1021/acsnano.9b06180>
75. G. Liu, J. Shen, Q. Liu, G. Liu, J. Xiong, J. Yang, W. Jin, Ultrathin two-dimensional MXene membrane for pervaporation desalination. *J. Memb. Sci.* **548**, 548–558 (2018). <https://doi.org/10.1016/j.memsci.2017.11.065>
76. O. Salim, K.A. Mahmoud, K.K. Pant, R.K. Joshi, Introduction to MXenes: synthesis and characteristics. *Mater. Today Chem.* **14**, 100191 (2019). <https://doi.org/10.1016/j.mtchem.2019.08.010>
77. M. Alhabeab, K. Maleski, B. Anasori, P. Lelyukh, L. Clark, S. Sin, Y. Gogotsi, Guidelines for synthesis and processing of two-dimensional titanium carbide ($\text{Ti}_3\text{C}_2\text{T}_x$ MXene). *Chem.*

- Mater. **29**, 7633–7644 (2017). <https://doi.org/10.1021/acs.chemmater.7b02847>
78. M. Khazaei, A. Ranjbar, K. Esfarjani, D. Bogdanovski, R. Dronskowski, S. Yunoki, Insights into exfoliation possibility of MAX phases to MXenes. *Phys. Chem. Chem. Phys.* **20**, 8579–8592 (2018). <https://doi.org/10.1039/C7CP08645H>
79. V. Natu, J.L. Hart, M. Sokol, H. Chiang, M.L. Taheri, M.W. Barsoum, Edge capping of 2D-MXene Sheets with poly-anionic salts to mitigate oxidation in aqueous colloidal suspensions. *Angew. Chem. Int. Ed.* **131**, 12655–12660 (2019). <https://doi.org/10.1002/ange.201906138>
80. F. Han, S. Luo, L. Xie, J. Zhu, W. Wei et al., Boosting the yield of MXene 2D sheets via a facile hydrothermal-assisted intercalation. *ACS Appl. Mater. Interfaces.* **11**, 8443–8452 (2019). <https://doi.org/10.1021/acsami.8b22339>
81. X. Yu, X. Cai, H. Cui, S.-W. Lee, X.-F. Yu, B. Liu, Fluorine-free preparation of titanium carbide MXene quantum dots with high near-infrared photothermal performances for cancer therapy. *Nanoscale* **9**, 17859–17864 (2017). <https://doi.org/10.1039/C7NR05997C>
82. M. Khazaei, A. Mishra, N.S. Venkataramanan, A.K. Singh, S. Yunoki, Recent advances in MXenes: from fundamentals to applications. *Curr. Opin. Solid State Mater. Sci.* **23**, 164–178 (2019). <https://doi.org/10.1016/j.cossms.2019.01.002>
83. Y. Zhang, L. Wang, N. Zhang, Z. Zhou, Adsorptive environmental applications of MXene nanomaterials: a review. *RSC Adv.* **8**, 19895–19905 (2018). <https://doi.org/10.1039/C8RA03077D>
84. W. Mu, S. Du, X. Li, Q. Yu, H. Wei, Y. Yang, S. Peng, Removal of radioactive palladium based on novel 2D titanium carbides. *Chem. Eng. J.* **358**, 283–290 (2019). <https://doi.org/10.1016/j.cej.2018.10.010>
85. J. Guo, Q. Peng, H. Fu, G. Zou, Q. Zhang, Heavy-metal adsorption behavior of two-dimensional alkalization-intercalated MXene by first-principles calculations. *J. Phys. Chem. C* **119**, 20923–20930 (2015). <https://doi.org/10.1021/acs.jpcc.5b05426>
86. G. Zou, J. Guo, Q. Peng, A. Zhou, Q. Zhang, B. Liu, Synthesis of urchin-like rutile titania carbon nanocomposites by iron-facilitated phase transformation of MXene for environmental remediation. *J. Mater. Chem. A* **4**, 489–499 (2016). <https://doi.org/10.1039/C5TA07343J>
87. Y.-J. Zhang, Z.-J. Zhou, J.-H. Lan, C.-C. Ge, Z.-F. Chai, P. Zhang, W.-Q. Shi, Theoretical insights into the uranyl adsorption behavior on vanadium carbide MXene. *Appl. Surf. Sci.* **426**, 572–578 (2017). <https://doi.org/10.1016/j.apsusc.2017.07.227>
88. I. Ihsanullah, MXenes (two-dimensional metal carbides) as emerging nanomaterials for water purification: Progress, challenges and prospects. *Chem. Eng. J.* **388**, 124340 (2020). <https://doi.org/10.1016/j.cej.2020.124340>
89. L. Fu, Z. Yan, Q. Zhao, H. Yang, Novel 2D Nanosheets with potential applications in heavy metal purification: a review. *Adv. Mater. Interfaces* **5**, 1801094 (2018). <https://doi.org/10.1002/admi.201801094>
90. A. Sinopoli, Z. Othman, K. Rasool, K.A. Mahmoud, Electro-catalytic/photocatalytic properties and aqueous media applications of 2D transition metal carbides (MXenes). *Curr. Opin. Solid State Mater. Sci.* **23**, 100760 (2019). <https://doi.org/10.1016/j.cossms.2019.06.004>